

Comparative properties of the interior and blowoff plasmas in a dynamic hohlraum

J. P. Apruzese, R. W. Clark, and J. Davis

Plasma Physics Division, Naval Research Laboratory, Washington, D.C. 20375

T. W. L. Sanford, T. J. Nash, and R. C. Mock

Sandia National Laboratories, Albuquerque, New Mexico 87185

D. L. Peterson

Los Alamos National Laboratory, Los Alamos, New Mexico 87545

(Received 2 February 2007; accepted 28 February 2007; published online 20 April 2007)

A Dynamic Hohlraum (DH) is formed when arrays of tungsten wires driven by a high-current pulse implode and compress a cylindrical foam target. The resulting radiation is confined by the wire plasma and forms an intense, $\sim 200\text{--}250$ eV Planckian x-ray source. The internal radiation can be used for indirect drive inertial confinement fusion. The radiation emitted from the ends can be employed for radiation flow and material interaction studies. This external radiation is accompanied by an expanding blowoff plasma. We have diagnosed this blowoff plasma using K-shell spectra of Mg tracer layers placed at the ends of some of the Dynamic Hohlraum targets. A similar diagnosis of the interior hohlraum has been carried out using Al and Mg tracers placed at 2 mm depth from the ends. It is found that the blowoff plasma is about 20–25% as dense as that of the interior hohlraum, and that its presence does not significantly affect the outward flow of the nearly Planckian radiation field generated in the hohlraum interior. However, the electron temperature of the blowoff region, at ~ 120 eV, is only about half that of the interior hohlraum plasma. © 2007 American Institute of Physics. [DOI: 10.1063/1.2718907]

I. INTRODUCTION

A Dynamic Hohlraum (DH) is an intense, nearly Planckian x-ray source that has been designed and demonstrated during the past few years using Sandia National Laboratories' Z facility.^{1–13} This source consists of an array or arrays of tungsten wires that implode onto a low atomic number cylindrical foam target. The DH, an excellent realization of an x-ray blackbody source, can be used for fundamental radiation transport studies and for inertial confinement fusion experiments^{14–16} using indirect drive.

A typical DH target consists of an 8–10 mm long, 5 mm diameter cylindrical CH₂ foam, surrounded by and coaxial with two nested arrays of tungsten wires. The wire arrays implode onto the foam target, compress it, and contain the x-ray radiation generated within and scattered by the foam plasma. Reliable diagnosis of the properties of DH's and their relationship to basic experimental conditions (target configuration, current, etc.) is critical to further improvements in these sources. An example of the value of such a diagnostic is that asymmetry in the x-ray power emitted from the ends of the hohlraum has been shown, in part by use of spectroscopic tracers, to be due to tungsten plasma obstructing the bottom of the target.^{11,17,18} This has been accomplished in DH experiments on "Z" by embedding layers of Al and/or Mg in the CH₂ foam target. The simple and well-understood atomic physics of the hydrogen- and helium-like K-shell ionization stages of these two elements provide the basis of spectroscopic diagnosis of the interior hohlraum. In previous experiments, tracers have been successfully employed to investigate the implosion dynamics of Z pinches

created by gas puffs¹⁹ and wire array²⁰ loads, as well as DHs.²¹

II. EXPERIMENTS

The cylindrical foam in the DH target is of density 14 mg cm⁻³, representing an uncompressed carbon atom density of $\sim 6 \times 10^{20}$ cm⁻³. Thin "pancake" circular tracer layers are embedded either at the ends of the target or within the target at 2 mm from the ends. Mg is included as 0.6 μm of MgF₂, which represents the same column density of Mg as for Al in the 0.3 μm of elemental Al which is used in the Al-bearing layers. Mg and Al have been used either alone or together depending on the particular shot. In most cases, the interior layer is Al, the end tracer layer, Mg. Implosion time is typically ~ 112 ns, with a peak radial x-ray power (defined to occur at "stagnation" time) of ~ 140 TW. The peak axial power, emanating from radiation exit holes at the ends of the target, is usually in the 8–15 TW range and occurs about 3 ns prior to stagnation. Peak axial power is preceded by the collision of the outer and inner tungsten wire arrays at about 21 ns prior to stagnation, and also by the impact of the wire plasma with the outer radial edge of the foam at about 6.5 ns before stagnation. A diagram of the experimental setup and diagnostic instruments is given in Fig. 1.

III. BASIS OF THE TRACER DIAGNOSTIC

The method and underlying principles governing the use of the interior tracer layers to diagnose DH's have been presented in detail in Refs. 10–12. Here we describe the method used for the end tracer spectra, which is somewhat different

TABLE I. Incident radiation temperatures, electron temperatures, in eV, and carbon ion densities, in 10^{21} cm^{-3} , for the blowoff plasma. They were inferred from analysis of K-shell absorption spectra of Mg tracers placed at the bottom end of the cylindrical hohlraum target, as discussed in the text. Also shown are the averages and standard deviations of the means.

Shot	Time (ns)	T_{rad}	T_e	N (carbon)
Z1299	-3.2	150	125	0.3
Z1299	-1.2	200	100	0.5
Z1299	integrated	225	125	1.1
Z1303	-3.6	300	100	1.1
Z1303	-1.6	175	150	0.5
Z1303	integrated	200	175	1.1
Z1430	integrated	250	100	1.4
Z1431	integrated	250	100	1.1
Z1438	integrated	175	125	1.4
Z1439	integrated	175	125	0.8
Z1440	integrated	225	100	1.1
Averages		211 ± 13	120 ± 7	0.95 ± 0.11

for calculating the various atomic rate coefficients can be found in Refs. 22–24.

The inference of the hohlraum plasma temperature and density is done by comparing the measured K-shell tracer spectrum (containing lines of Al, or Mg, or both) to a table of precalculated intensities. We obtain the statistically most probable plasma conditions as follows. The table of line intensities is calculated for a range of assumed electron temperatures, ion densities, and radiation (of temperature T_{rad}) incident on the blowoff plasma. The incident radiation arises from the denser interior hohlraum plasma, which has not expanded from its original location, as has the blowoff plasma. For each entry in the table, the calculated intensities are compared with the experimental values for a particular spectrum. This comparison produces a χ^2 measure of goodness of fit^{25,26} for each of the calculated spectra. The minimum χ^2 determines which calculated spectrum and associated conditions are the best fit. χ^2 is defined as

$$\chi^2 = \sum_n \frac{(I_n - M_n)^2}{\sigma_n^2}, \quad (1)$$

where M_n is the measured intensity of the n th line, I_n is the calculated intensity of the line, and σ_n is the estimated experimental uncertainty of the measured line intensity. Equation (1) treats each set of calculated intensities as a “parent distribution,” and weighs those lines that are measured most accurately the greatest in determining which “parent distribution,” i.e., set of assumed plasma conditions, is most probable. The experimental uncertainty σ_n in measuring the line intensity is mostly due to the presence of background noise such as that seen in the spectrum of Fig. 2. The quantity σ_n is an estimate of how accurately the area within the line profile can be extracted through the noise. Values of σ_n typically range from 10 to 70% of the line intensity, averaging about 30%.

The table consists of sets of Mg K-shell line intensities calculated for the three-dimensional parameter space of electron temperature T_e , incident radiation temperature T_{rad} , and

the carbon ion density, referring in each case to the position of the tracer in the blowoff plasma. The nine assumed electron and incident radiation temperatures are 100, 125, 150, 175, 200, 225, 250, 275, and 300 eV. There are 26 assumed carbon ion densities, ranging in increments of $\sim 30\%$ from $1.0 \times 10^{20} \text{ cm}^{-3}$ to $7.2 \times 10^{22} \text{ cm}^{-3}$ (the carbon atom density of the cold foam is $6 \times 10^{20} \text{ cm}^{-3}$). Therefore, the total number of distinct plasma conditions for which line intensities have been calculated and tabulated is $9 \times 9 \times 26 = 2106$. The overall accuracy of the modeling and fitting procedure is discussed in detail in Ref. 11. Sources of error include the granularity of the table, uncertainties in the underlying atomic rates, and the inherent simplification of a one-dimensional radiation transport model. We estimate the overall model-related uncertainty in the inferred temperatures to be 20–30 eV, to which must be added the shot-to-shot variation in the temperatures deduced from the experimental data.

V. RESULTS AND DISCUSSION

The results derived from analyzing 11 spectra from end tracers (all from the bottom side of the target, and all Mg) are presented in Table I. The criteria used in selecting these spectra are as follows: at least two tracer lines must be present, uncontaminated by tungsten emission. The spectra are either time-resolved within ~ 2 ns of peak axial power, or time-integrated. Placing the time-integrated spectra on the same footing as those time-resolved near peak power is justified by the fact that, as discussed in Ref. 11, the time-integrated spectra are dominated by the emission near peak power. The average inferred radiation temperature incident on the blowoff region, 211 ± 13 eV, exceeds the mean local electron temperature of 120 ± 7 eV by nearly a factor of 2. This is reflective of the fact that the radiation field is largely produced by the hotter, denser hohlraum plasma a few mm distant, but the local kinetic temperature has been reduced by the effects of hydrodynamic expansion and radiative cooling. The diagnosed carbon ion density of $(9.5 \pm 1.1) \times 10^{20} \text{ cm}^{-3}$ is only

TABLE II. Hohlraum radiation and electron temperatures, in eV, inferred from Al and/or Mg tracer layers placed 2 mm from the ends at the tops or bottoms of the targets as indicated. Diagnosed carbon ion densities (in 10^{21} cm^{-3}) are also given, as are the averages and standard deviations of the means.

Shot T/B	Time (ns)	T_{rad}	T_e (inner)	T_e (outer)	N (carbon)
Z1022 T	-3.5	172	200	175	2.3
Z1022 T	-1.5	185	225	175	2.3
Z1023 T	-4	219	250	200	11.4
Z1023 T	-2	259	300	250	11.4
Z1023 T	integrated	208	225	200	4.0
Z1023 B	-4.3	209	325	200	2.3
Z1023 B	-2.3	206	250	200	6.7
Z1025 T	-3.3	168	175	175	3.0
Z1025 T	-1.3	173	200	175	2.3
Z1025 T	integrated	177	200	175	5.1
Z1025 B	-1.5	192	275	175	2.3
Z1025 B	integrated	177	200	175	2.3
Z1132 T	integrated	238	350	250	3.0
Z1132 B	integrated	234	250	225	8.7
Z1246 T	integrated	211	275	200	3.0
Z1246 B	integrated	190	300	175	1.8
Z1303 B	-3.6	199	250	150	2.3
Z1430 B	integrated	205	275	175	3.0
Z1431 B	integrated	221	300	175	3.0
Z1438 B	integrated	217	275	175	3.0
Z1439 B	integrated	187	200	175	8.7
Z1440 B	integrated	184	250	150	2.3
Z1598 T	integrated	169	250	125	1.8
Z1598 B	integrated	187	250	150	2.3
Z1600 B	integrated	183	225	150	3.0
Averages		199 ± 5	251 ± 9	182 ± 6	4.1 ± 0.6

slightly greater than the corresponding cold target carbon atom density of $6 \times 10^{20} \text{ cm}^{-3}$. This is the result of two opposing processes: the compression of the foam target by the tungsten arrays on the one hand, and the relatively free expansion of the blowoff region on the other.

It is of interest to compare these results from the end tracer spectroscopic analyses with those obtained from the interior tracers. Some of the interior tracer spectra have been previously presented, and results from analyzing them are discussed in Refs. 10–12. Table II presents an update that includes all 25 spectra (through shot Z1600) that meet the criteria defined above. The expanded group of interior tracer results presented in Table II continues to reveal no evidence of any difference between the temperatures of the radiation fields emitted from the tops and bottoms of the hohlraums. The average top-to-bottom temperature ratio is 1.03 ± 0.05 , where 0.05 is the standard deviation of the mean. This ratio is derived from the seven instances listed in Table II in which top and bottom spectra were either collected nearly simultaneously, or time-integrated on the same shot.

The interior tracer spectral analyses include the inference of an axial electron temperature profile, as discussed in Ref. 10. The end points of the deduced profiles are labeled as $T_e(\text{inner})$ and $T_e(\text{outer})$ in Table II, and their average values are plotted in Fig. 3 along with the average electron temperature in the blowoff region inferred from the end tracer spec-

tra. Also plotted in Fig. 3 are two axial temperature profiles obtained from a two-dimensional radiation magnetohydrodynamics (MRHD) simulation.²⁷ The two calculated profiles arise from different models of the tungsten array-foam interface and are referred to as “rough” and “smooth” in Fig. 3. The “rough” model develops more inhomogeneities at the interface by postulating a more rapid foam expansion than the baseline “smooth” case. These different interface models are discussed in Ref. 7. The higher calculated temperatures arising from the “rough” model are due to the enhanced inhomogeneities impeding axial radiation flow out of the hohlraum, inhibiting radiative cooling relative to the “smooth” case. Importantly, all three comparison points shown in Fig. 3 indicate agreement, within the estimated uncertainties, of the experimentally inferred temperature with at least one of the calculated profiles. Marginally, however, the experimental data suggest that the temperature gradient may be somewhat less steep than calculated.

In the analyses of both the end and interior tracer spectra, a spatially constant density has been assumed. The results given in Tables I and II indicate that the ratio of the blowoff plasma density to that of the hohlraum interior is 0.23 ± 0.04 . This means that the blowoff region is likely to be far less optically thick than the interior of the hohlraum. If the axially streaming, nearly blackbody radiation from the interior were being absorbed and re-emitted by the cooler

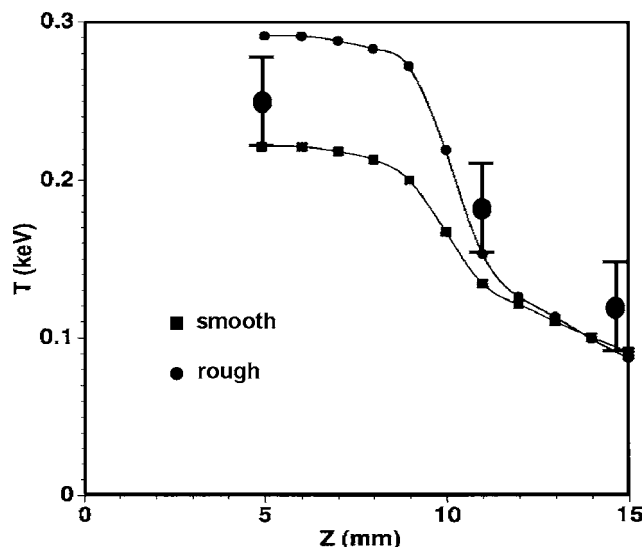


FIG. 3. Comparison of electron temperatures inferred from the interior and end tracers near peak power, with those obtained in 2D RMHD calculations. Two different models of the tungsten/ CH_2 interface are denoted by “smooth” and “rough.” The inferred interior tracer temperatures are based on the mean from 25 experimental spectra (Table II); the end tracer temperature is based on the mean from 11 spectra (Table I).

plasma expanding from the ends of the compressed target, a far lower radiation temperature would be inferred from the end tracer spectra than from the interior tracers. According to Tables I and II, the difference in T_{rad} as diagnosed from the interior versus end tracers is only 12 eV, well within the estimated uncertainty of the method. This result enhances our confidence in the diagnostic method and in our overall understanding of the radiation physics and hydrodynamics of the Dynamic Hohlraum.

In summary, key properties of the interior and blowoff plasmas of Dynamic Hohlräume created on Sandia National Laboratories’ Z generator have been diagnosed by analyzing spectra from Al and/or Mg tracer layers that were placed either at the ends of the hohlraum target or 2 mm deep in its interior. The results, in conjunction with two-dimensional MRHD simulations, demonstrate a fundamental understanding of both the radiation physics and hydrodynamics of these unique x-ray sources. The radiation temperature created by the dense interior hohlraum plasma is the same as that seen by the blowoff plasma several mm away, which indicates that the expanding exterior plasma does not “spoil” the intense axial radiation field by absorbing and re-emitting it at a far lower temperature. The deduced electron temperature profile compares well with simulations, although the data marginally indicate a somewhat shallower profile than that calculated.

In future work, the effects of density gradients and the effects of radial gradients in the electron temperature need to be investigated. It is possible that a different kind of tracer could be used to infer radial temperature gradients. To accomplish this would require that donut-shaped layers of Al and/or Mg be included in the foam during fabrication. To

avoid the opacity of the overlying tungsten, such a tracer would likely have to be viewed axially, but its absorption lines would presumably reflect conditions within a limited radial range.

ACKNOWLEDGMENTS

The application of aluminum and magnesium tracers to hohlräume was demonstrated in experiments performed by Dr. J. E. Bailey of Sandia National Laboratories. We thank Dr. R. J. Leeper for programmatic support.

This work was supported by Sandia National Laboratories.

- ¹J. H. Brownell, R. L. Bowers, K. D. McLenithan, and D. L. Peterson, *Phys. Plasmas* **5**, 2071 (1998).
- ²T. J. Nash, M. S. Derzon, G. A. Chandler *et al.*, *Phys. Plasmas* **6**, 2023 (1999).
- ³R. J. Leeper, T. E. Alberts, J. R. Asay *et al.*, *Nucl. Fusion* **39**, 1283 (1999).
- ⁴T. W. L. Sanford, R. E. Olson, R. L. Bowers *et al.*, *Phys. Rev. Lett.* **83**, 5511 (1999).
- ⁵T. W. L. Sanford, R. E. Olson, R. C. Mock *et al.*, *Phys. Plasmas* **7**, 4669 (2000).
- ⁶J. E. Bailey, G. A. Chandler, S. A. Slutz *et al.*, *Phys. Rev. Lett.* **89**, 095004 (2002).
- ⁷T. W. L. Sanford, R. W. Lemke, R. C. Mock *et al.*, *Phys. Plasmas* **9**, 3573 (2002).
- ⁸T. W. L. Sanford, R. W. Lemke, R. C. Mock, and D. L. Peterson, *Phys. Plasmas* **10**, 3252 (2003).
- ⁹T. W. L. Sanford, R. C. Mock, S. A. Slutz, and D. L. Peterson, *Phys. Plasmas* **10**, 4790 (2003).
- ¹⁰J. P. Apruzese, R. W. Clark, P. C. Kepple, J. Davis, T. W. L. Sanford, T. J. Nash, R. C. Mock, and D. L. Peterson, *Phys. Plasmas* **12**, 012705 (2005).
- ¹¹T. W. L. Sanford, T. J. Nash, R. C. Mock, J. P. Apruzese, and D. L. Peterson, *Phys. Plasmas* **13**, 012701 (2006).
- ¹²J. P. Apruzese, R. W. Clark, J. Davis, T. W. L. Sanford, T. J. Nash, R. C. Mock, and D. L. Peterson, *Rev. Sci. Instrum.* **77**, 10F303 (2006).
- ¹³J. E. Bailey, G. A. Chandler, R. C. Mancini *et al.*, *Phys. Plasmas* **13**, 056301 (2006).
- ¹⁴J. E. Bailey, G. A. Chandler, S. A. Slutz *et al.*, *Phys. Rev. Lett.* **92**, 085002 (2004).
- ¹⁵C. L. Ruiz, G. W. Cooper, S. A. Slutz *et al.*, *Phys. Rev. Lett.* **93**, 015001 (2004).
- ¹⁶S. A. Slutz, K. J. Peterson, R. A. Vessey *et al.*, *Phys. Plasmas* **13**, 102701 (2006).
- ¹⁷T. W. L. Sanford, R. C. Mock, R. J. Leeper *et al.*, *Phys. Plasmas* **10**, 1187 (2003).
- ¹⁸T. W. L. Sanford, T. J. Nash, R. C. Mock, D. L. Peterson, R. G. Watt, R. E. Chrien, J. P. Apruzese, R. W. Clark, N. F. Roderick, G. S. Sarkisov, and M. G. Haines, *Phys. Plasmas* **12**, 022701 (2005).
- ¹⁹H. Sze, P. L. Coleman, B. H. Failor *et al.*, *Phys. Plasmas* **7**, 4223 (2000).
- ²⁰C. Deeney, J. P. Apruzese, C. A. Coverdale, K. G. Whitney, J. W. Thornhill, and J. Davis, *Phys. Rev. Lett.* **93**, 155001 (2004).
- ²¹J. E. Bailey, G. A. Chandler, G. A. Rochau, Y. Maron, S. A. Slutz, G. S. Dunham, I. Golovkin, P. W. Lake, R. W. Lemke, J. M. Lucas, J. J. MacFarlane, T. A. Mehlhorn, T. C. Moore, D. G. Schroen, E. Stambulchik, and K. Youngblood, *High energy density physics* **1**, 21 (2005).
- ²²J. P. Apruzese, K. G. Whitney, J. Davis, and P. C. Kepple, *J. Quant. Spectrosc. Radiat. Transf.* **57**, 41 (1997).
- ²³J. P. Apruzese, P. E. Pulsifer, J. Davis *et al.*, *Phys. Plasmas* **5**, 4476 (1998).
- ²⁴D. Duston and J. Davis, *Phys. Rev. A* **23**, 2602 (1981).
- ²⁵H. D. Young, *Statistical Treatment of Experimental Data* (McGraw-Hill, New York, 1962), pp. 80–87 and 101–108.
- ²⁶J. Mandel, *The Statistical Analysis of Experimental Data* (Dover, New York, 1984) pp. 234–240.
- ²⁷D. L. Peterson, R. L. Bowers, J. H. Brownell *et al.*, *Phys. Plasmas* **3**, 368 (1996).